Ultrasound in Med. & Biol., Vol. 46, No. 11, pp. 3032–3045, 2020

0301-5629/$ - see front matter

https://doi.org/10.1016/j.ultrasmedbio.2020.07.004

● *Original Contribution*

ULTRASOUND-MEDIATED DELIVERY OF CHEMOTHERAPY INTO THE TRANSGENIC ADENOCARCINOMA OF THE MOUSE PROSTATE MODEL

Stein-Martin T. Fagerland,[*,†] Sigrid Berg,[†,‡,§] Deborah K. Hill,[†] Sofie Snipstad,[*,§,¶] Einar Sulheim,[*,§,¶] Astrid Hyldbakk,[*,¶] Jana Kim,[†] and Catharina de Lange Davies[*]

[*] Department of Physics, Norwegian University of Science and Technology, Trondheim, Norway; [†] Department of Circulation and Medical Imaging, Norwegian University of Science and Technology, Trondheim, Norway; [‡] Department of Health Research, SINTEF Digital, Trondheim, Norway; [§] Cancer Clinic, St. Olav's Hospital, Trondheim, Norway; and [¶] Department of Biotechnology and Nanomedicine, SINTEF Industry, Trondheim, Norway

(*Received* 8 *February* 2020; *revised* 19 *June* 2020; *in final from* 7 *July* 2020)

Abstract—Ultrasound (US) in combination with microbubbles (MB) has had promising results in improving delivery of chemotherapeutic agents. However, most studies are done in immunodeficient mice with xenografted tumors. We used two phenotypes of the spontaneous transgenic adenocarcinoma of the mouse prostate (TRAMP) model to evaluate if US + MB could enhance the therapeutic efficacy of cabazitaxel (Cab). Cab was either injected intravenously as free drug or encapsulated into nanoparticles. In both cases, Cab transiently reduced tumor and prostate volume in the TRAMP model. No additional therapeutic efficacy was observed combining Cab with US + MB, except for one tumor. Additionally, histology grading and immunostaining of Ki67 did not reveal differences between treatment groups. Mass spectrometry revealed that nanoparticle encapsulation of Cab increased the circulation time and enhanced the accumulation in liver and spleen compared with free Cab. The therapeutic results in this spontaneous, clinically relevant tumor model differ from the improved therapeutic response observed in xenografts combining US + MB and chemotherapy. (E-mail: catharina.davies@ntnu.no)

Key Words: **Nanoparticle, Cabazitaxel, Ultrasound, Microbubbles, Drug delivery, Transgenic adenocarcinoma of the mouse prostate model, TRAMP model, Prostate cancer.**

INTRODUCTION

Prostate cancer is the third most deadly cancer among men in the European Union, with an estimated 107,300 deaths in 2018 (Ferlay et al. 2018). Thus, more efficient therapies are needed to improve prostate cancer survival. Nanoparticles (NP) and ultrasound combined with microbubbles (US + MB) are promising methods to increase the delivery and efficacy of chemotherapeutic drugs. Through encapsulation of drugs in NP, the pharmacokinetic properties can be altered to improve efficacy and reduce adverse effects (Peer et al. 2007). NP have had promising results in pre-clinical studies (Fusser et al. 2019), and the improvement to treatment response has been attributed to the enhanced permeability and retention effect (EPR effect), where NP target tumors because of leaky tumor capillaries and are retained there because of the lack of effective lymphatic drainage (Maeda et al. 2000). However, a recent study strongly argued that NP are transported actively in transcellular processes, rather than passively through gaps between endothelial cells (Sindhwani et al. 2020). NP delivery to tumors has been limited by biological barriers hindering the NP from reaching the cancer cells (Lammers et al. 2012; Rosenblum et al. 2018; Ding et al. 2019). A review of NP delivery to tumors indicated that only a median of 0.7% of injected NP reached the tumor (Wilhelm et al. 2016). US + MB-mediated drug delivery is one method to improve NP delivery (Tharkar et al. 2019). US + MB-mediated drug delivery is known by many terms, including sonopermeation (Snipstad et al. 2018). Sonopermeation effects are mediated by acoustic radiation force, which causes a fluid stream in the direction of the US pulse, and cavitation, which is the creation and oscillation of bubbles in the acoustic field. These effects might lead to changes in tumor perfusion,

Address correspondence to: Catharina de Lange Davies, Ph.D., Norwegian University of Science and Technology, Trondheim, Norway. E-mail: catharina.davies@ntnu.no

enhanced vascular permeability and facilitated transport of drugs through the extracellular matrix toward cancer cells. US + MB-mediated drug delivery has increased drug efficacy in both pre-clinical (Lin et al. 2012; Kotopoulis et al. 2014. Snipstad et al. 2017) and clinical (Carpentier et al. 2016; Dimcevski et al. 2016; Wang et al. 2018; Mainprize et al. 2019) studies. In addition, there are several ongoing clinical trials assessing the effect of US + MB combined with chemotherapy or monoclonal antibodies on either pancreatic cancer (ClinicalTrials.gov identifier NCT04146441); liver metastases from colorectal, pancreatic or breast cancer (ClinicalTrials.gov identifier NCT02233205, NCT03458975 and NCT03477019); brain metastases from malignant melanoma (ClinicalTrials.gov identifier NCT04021420); and in combination with neoadjuvant chemotherapy for breast cancer (ClinicalTrials.gov identifier NCT03385200).

Most pre-clinical studies of the treatment efficacy of drug-loaded NP alone or combined with US + MB have been conducted in immunodeficient xenograft cancer models in mice, which differ from human cancer in several respects: The tumor develops from cells that are already malignant, leading to less heterogenous cancer genetics; the mice are immunodeficient, thus diminishing the anti-cancer role of the immune system (Zitvogel et al. 2016); and the cancer cells are often grown outside of their tissue of origin, preventing interplay between the cancer cells and the organ-specific connective tissue (Parisotto and Metzger 2013; Day et al. 2015; Gengenbacher et al. 2017). The use of genetically engineered cancer models can address these shortcomings. The transgenic adenocarcinoma of the mouse prostate (TRAMP) is a commonly used spontaneous prostate cancer model in which cancer develops from normal prostate cells that transition through dysplastic stages before they become malignant (Greenberg et al. 1995; Gingrich et al. 1996). The TRAMP model has been used mainly to examine cancer preventive effects of interventions, ranging from the efficacy of diets (Liu et al. 2019) and supplements of silibinin (Raina et al. 2008) or selen (Wang et al. 2009), to some types of drugs, for example, non-steroidal anti-inflammatory drugs (Silva et al. 2018) and tyrosine kinase inhibitors (Da Silva et al. 2020). In studies of cancer prevention, the treatment is administered from early in life, before the onset of cancer. Studies of the anti-cancer efficacy of chemotherapeutic agents should start later in life, once the disease has developed, as reported in a few studies using the TRAMP model (Degrassi et al. 2007; Sogaard et al. 2018).

In this study, we investigated if NP encapsulation and US + MB could enhance the therapeutic efficacy of cabazitaxel (Cab) in two phenotypes of the TRAMP model. In the TRAMP model, a subgroup develops poorly differentiated (PD) tumors, whereas the majority develop a dysplastic prostate with a high-grade prostatic intraepithelial neoplasia (PIN). The therapeutic response was thus evaluated either by the volume of the tumor (PD group) or by the volume of the prostate (PIN group). In addition, the effect of NP encapsulation and US + MB on biodistribution of Cab was assessed using mass spectrometry (MS). To our knowledge, this is the first time a study has been conducted in the TRAMP model using Cab and NP-encapsulated Cab alone or in combination with US + MB.

METHODS

Animal model

All animal experiments were approved by the Norwegian Food Safety Authority. TRAMP mice were purchased from Jackson Laboratories in 2012 and used to establish an in-house colony at the Norwegian University of Science and Technology (NTNU, Trondheim, Norway). Mice heterozygous for the TRAMP mutation were bred using homozygous females from the in-house colony and C57BL6 males purchased from Charles River Germany (Sulzfeld, Germany). The presence of TRAMP mutation was verified using polymerase chain reaction. Mice were housed under specific pathogen-free conditions, in groups of one to six, in individually ventilated cages (Model 1284 L, Tecniplast, Lyon, France) at temperatures from 21°C−23°C, with 45%−60% relative humidity, 70 air changes per hour, 12-h light/dark cycle and *ad libitum* access to food and sterile water. They were fed RM1 expanded pellets (Special Diets Services, Essex, UK), and the cages were enriched with housing, nesting material and gnaw sticks. Mice were euthanized if they were moribund, displayed signs of excessive scratching or had a weight loss >10% or a tumor diameter >15 mm. Approximately 20% of TRAMP mice bred in a C57BL6 background strain develop fast-growing PD tumors in their lifetime, starting from around 16 wk of age, but also appearing after 20 wk of age (Chiaverotti et al. 2008; Fagerland et al. 2020). After 20 wk of age, around 90% of TRAMP mice in the C57BL6 will have severe dysplasia with cribriform patterns (Chiaverotti et al. 2008). The prostate volume also increases with age well after 20 wk of age (Hill et al. 2016). For these reasons, we chose to screen for PD tumors in the TRAMP mice from 16 wk of age and to treat PD tumors when they appeared. Treatment of mice without PD tumors was started at 25 wk of age, when the grade of dysplasia was high, prostate volumes large and most PD tumors already detected.

Ultrasound imaging and screening

To separate the TRAMP mice with fast-growing PD tumors from the mice with a dysplastic prostate, mice were screened with US imaging as described earlier

(Fagerland et al. 2020). Imaging was performed with a Vevo 3100 scanner (FUJIFILM Visualsonics, Toronto, ON, Canada) and an MX550 D probe with 40-MHz center frequency, giving a 30×30-μm^2 in-plane resolution and 80-μm through-plane resolution. Three-dimensional images were acquired by imaging every 76 μm using a 3-D motor. Mice were anesthetized with 1.5%−2.5% isoflurane with 0.5 L/min 5:1 air:O_2 mix. The isoflurane dose was adjusted to reach a target respiratory rate of 80 breaths/min. Mice were restrained in supine position by taping the hind limbs to the imaging stage. To remove fur, the mice were shaved with an electric razor followed by application of depilation creme. US imaging gel was used to secure good acoustic contact between the transducer and the mouse skin. Mice were screened one to three times at an age ranging from 16−24 wk. If a PD tumor was detected with US, the mouse was imaged with magnetic resonance imaging (MRI) the next day to verify the findings, upon which the mouse was treated the same week or the week after if PD tumor volume was <30 mm^3. The MRI protocol is the same as that used for treatment monitoring and is described below.

Treatment groups

Mice with PD tumors were available in limited numbers and were divided into three treatment groups to examine the therapeutic effect of Cab and Cab combined with ultrasound and microbubbles (US + MB):

1. Control (Ctrl): No treatment
2. Cabazitaxel (Cab): 10 mg/kg Cab once a week for 3 wk
3. Cab combined with US and MB (Cab−US + MB): 10 mg/kg Cab once a week for 3 wk combined with US + MB

Mice without PD prostate tumors were divided into five different groups, examining the therapeutic effect of Cab and NP with and without US + MB:

1. Control (Ctrl): No treatment
2. Cab: 10 mg/kg Cab once a week for 3 wk.
3. Cab combined with US and MB (Cab−US + MB): 10 mg/kg Cab once a week for 3 wk combined with US + MB.
4. Nanoparticles (NP): 10 mg/kg Cab encapsulated in NP once a week for 3 wk.
5. NP combined with US and MB (NP−US + MB): 10 mg/kg Cab encapsulated in NP once a week for 3 wk combined with US + MB.

Cab and NP

Cab is approved as a second-line treatment in metastatic prostate cancer and is a good candidate for polymeric NP encapsulation as its high toxicity makes altered biodistribution and pharmacokinetics favorable. Cab (Biochempartner Co. Ltd., Wuhan, Hubei, China) was dissolved to 40 mg/mL in distilled water with 1040 mg/mL Tween-80 (Sigma-Aldrich, St. Louis, MO, USA) and stored at +4°C. On each day of the experiment, Cab was diluted 1:4 in 13% ethanol and further diluted in 0.9% NaCl to 6 mg/mL concentration before intravenous injection. PEGylated poly(2-ethyl-butyl cyanoacrylate) NP loaded with Cab were synthesized as described previously (Snipstad et al. 2017). Cab concentration in the NP was measured by MS, and NP solution was diluted in 0.9% NaCl to a 6 mg/mL concentration of Cab, resulting in a NP concentration around 67 mg/mL. The mice received a weekly dose of 10 mg/kg Cab, either free or encapsulated in NP. The injected volume varied from 41−62 μL. Intravenous access was established by placing a 24G catheter (BD Neoflon, Becton Dickinson & Company, Franklin Lakes, NJ, USA) in the tail vein.

MRI-Guided US treatment

US treatment was done under MRI guidance, combining an RK100 (FUS Instruments, Toronto, ON, Canada) with a 7-T MRI scanner (Biospec 70/20 Avance III, Bruker Biospin MRI, Ettlingen, Germany). The RK100 consists of a water tank containing a three-axis positioning system with a US transducer and a control station with a PC, amplifier and signal generator. Approximately 8 L of deionized water was poured into the water tank and heated to approximately 40°C to reduce the amount of dissolved gas in the water and avoid hypothermia during treatment. On each day of treatment, the spatial coordinates of the US system and the MRI scanner were co-registered according to the instructions of the manufacturer.

MRI scans were acquired before US treatment to localize the tumor or prostate and determine which areas to treat. These magnetic resonance images were acquired using an 86-mm volume resonator coil for both radiofrequency (RF) transmission and reception. Axial T2-weighted coronal images were acquired with the following settings: TE 58.5 ms, TR 4000 ms, RARE factor 8, averages 6, in-plane resolution 0.2×0.2 mm^2, slice thickness 0.8 mm and acquisition time 6 min.

US treatment was performed using a single-element spherically curved transducer with center frequency 1.1 MHz, aperture 75 mm and focus at 60 mm. The US settings were a peak negative pressure of 0.55 MPa, resulting in a mechanical index of 0.5,

$$\text{peak negative pressure (MPa)} / \sqrt{\text{center frequency (MHz)}}$$

10,000 cycles and 3-min sonication time. Pulse repetition time varied depending on the area of tumor or prostate. In tumors, the mean number of treatment points was 10 (range: 6−14), covering an area of 50−117 mm^2

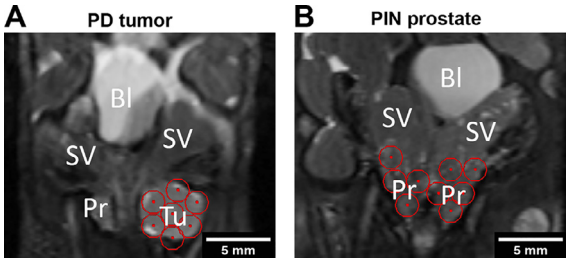

Fig. 1. Magnetic resonance images of representative examples of placement of ultrasound treatment areas (red circles) on the poorly differentiated tumors (A) and prostates with prostatic intraepithelial neoplasia (B). The individual treatment areas are 1.63 mm in diameter, corresponding to the full width at half-maximum for the radial pressure profile. Bl = bladder; Pr = prostate; SV = seminal vesicle; Tu = tumor.

(Fig. 1a). The mean pulse repetition time was 2.8 s (range: 1.8−3.5 s). In the treatment of prostates, the mean number of treatment points was 15 (range: 8−20) (Fig. 1b), covering an area of 67−167 mm^2. The mean pulse repetition time was 3.8 s (range: 2.2−4.8 s). All treatment points were selected at the same depth, as the axial pressure wave remained within −6 dB over 8.18 mm, giving good coverage in the anterior−posterior direction. The US contrast agent SonoVue (Bracco, Milan, Italy) was chosen as the MB in the described experiments and was prepared according to the manual supplied by the manufacturer. Mice received a bolus injection of 50 μL of undiluted SonoVue into the tail vein followed by sonication for 3 min. This was performed three times, resulting in a total injection volume of 150 μL and sonication time of 9 min per treatment. The treatment was repeated weekly for 3 wk. Figure 2 shows the treatment timeline for US + MB treatment sessions.

Treatment monitoring

The treatment response was monitored by measuring PD tumor volume or prostate volume with MRI. Imaging was done using a Bruker 7 T Biospec 70/20 Avance III scanner with an 86-mm volume resonator coil for RF transmission, and a phased array mouse heart surface coil was placed close to the lower abdomen for RF reception. Axial T2-weighted images were acquired with the settings TE 58.5 ms, TR 5000 ms, RARE factor 6, averages 6, in-plane resolution 0.1 × 0.1 mm^2, slice thickness 0.4 mm and acquisition time 10 min. Mice were kept under isoflurane gas anesthesia and were placed on the scanner bed in the prone position with a gauze and tape over the lower back to reduce motion from breathing. Mice with PD tumors were imaged weekly, and mice with PIN prostate were imaged every other week. MR images were exported as DICOM from Paravision 6.0.1 and loaded into FIJI ImageJ (Schindelin et al. 2012), where volumes were estimated based on manual segmentation of the image stacks. The ventral, lateral and dorsal prostate lobes were included in the segmentation. The anterior prostate lobes were not included as they are difficult to differentiate from the seminal vesicle because of their intertwined relationship. Søgaard et al. (2018) also chose to omit the anterior lobe.

Histology and immunohistochemistry

For a subgroup of mice without PD tumors, the treatment effect was also assessed with histology and immunohistochemistry. Thirty mice were included in the analysis, 3 per treatment group, and the analysis was performed 2 or 6 wk after the end of treatment. Mice were euthanized by cervical dislocation, and prostates harvested together with the seminal vesicle, bladder and urethra and fixed in 4% formaldehyde before paraffin embedding. Sectioning was done with a microtome (Leica RM2255, Leica Biosystems, Buffalo Grove, IL, USA), and the sections were stained for hematoxylin, erythrosine and saffron (HES) or the proliferation marker Ki-67 with a light hematoxylin counterstain.

Ki-67 staining was done using a Dako Autostainer (Agilent, Santa Clara, CA, USA). Sections were incubated with anti-Ki67 antibody (ab16667, clone SP6 1:50, Abcam, London, UK) for 40 min. After a rinse, the sections were washed in buffer and incubated for 30 min in

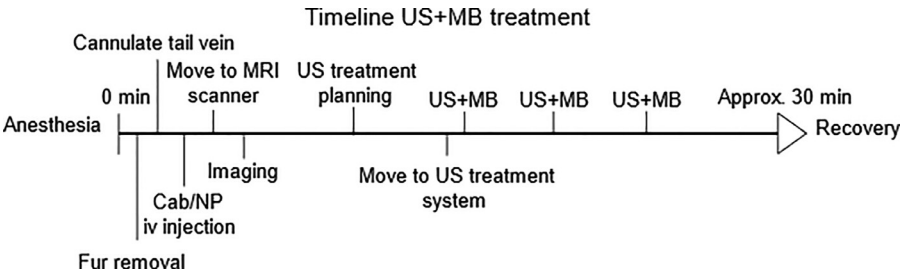

Fig. 2. Timeline of the treatment steps involved in US + MB treatment. The treatment was repeated weekly for 3 wk. Cab = cabazitaxel; MRI = magnetic resonance imaging; NP = nanoparticle; US + MB = ultrasound combined with microbubbles.

labeled polymer horseradish peroxidase anti-rabbit (Daco K4003, Agilent), using DAB (Dako K3468, Agilent) to develop the stain. In Sakura Tissue-Tek Prisma, the slides were lightly counterstained with hematoxylin. The stained sections were digitalized using a slide microscope (VS120-S5, Olympus, Tokyo, Japan). The proliferative index was quantified as the percentage of cells positive for Ki-67 marker and was calculated using QuPath software (Bankhead et al. 2017). Regions of interest were drawn over separate prostate lobes, and the number of Ki-67 positive cells was determined using the positive cell detection function. The prostates were fixed by preserving the whole structure, which made it difficult to determine the transition between dorsal lobe and anterior lobe when the PIN was high grade. Because of this, the inferior part of the dorsal lobe was used to score the dorsal lobe, and the anterior lobe was omitted from from HES grading and Ki-67 quantification.

The HES sections were graded using the TRAMP grading scheme by Berman-Booty et al. (2012). This grading scheme was chosen because the output is quantitative. The scheme grades lesions based on seven levels of severity (normal, three grades of PIN, phyllodes tumor and three grades of malignancy) and distribution (focal, multifocal or diffuse). The score is the sum of the most severe lesion and the most common lesion. The grading scheme differentiates high-grade PIN from well-differentiated adenocarcinoma by the presence of invasion, which requires invasion of epithelial cells into underlying smooth muscle and reactive fibroblasts and myoepithelial cells in the area of invasion.

Biodistribution of Cab

MS quantification of Cab was performed to assess the effect of NP encapsulation and US + MB on drug biodistribution. Twelve TRAMP mice in the age range 25−28 wk were included. Mice were imaged with US 2 d before the experiment to exclude mice with PD tumors. The mice were exposed to a single treatment equivalent to groups 5, 6, 7 and 8, and euthanized 2 h later. To quantify only Cab residing in the organ tissue and not include Cab content from the blood, all mice were perfused with phosphate-buffered saline (PBS). Euthanasia was performed by first anesthetizing the mouse with isoflurane and administering a lethal dose of pentobarbital intraperitoneally. After the mouse stopped breathing, the chest was opened, and a blood sample collected from the right ventricle. Further, an incision was made in the right atrium. Then a catheter was used to puncture the left ventricle and perfuse the mouse with 10 mL of PBS. After perfusion, the brain, heart, lung, liver, kidney, spleen, anterior prostate lobe, dorsolateral lobes and ventral lobe were harvested and frozen individually. Prostate lobes were separated using microdissection. All samples were lyophilized and weighed before and after lyophilization. The Cab content of the samples was extracted and quantified using a Agilent 1290 HPLC system coupled to an Agilent 6490 triple quadrupole MS, as described earlier (Sulheim et al. 2019).

Toxicity

Intravenous injection of NP led to instant apnea in all mice treated with NP. Heart rate and respiration rate were monitored during and after intravenous injection of NP in four mice, using a Vevo 3100 (FUJIFILM Visualsonics) system. Weight was recorded by weighing mice weekly during treatment and every other week after the end of treatment.

Statistical analysis

A two-way mixed analysis of variance was performed to evaluate if prostate volumes and weights significantly differed between treatment groups. A p value ≤ 0.05 was considered to indicate statistical significance.

RESULTS

TRAMP phenotype stratification

The TRAMP mice were screened to distinguish between mice with and without PD tumors (Fig. 3 contains representative images). Eighty-two TRAMP mice were screened for PD tumors, and 16 tumors were detected in the age range 17−25 wk. Two of the mice were euthanized because of tumor burden at the time of PD tumor detection, and 14 of the mice with PD tumors were included in treatment groups 1−3. Mice without PD tumors were expected to have prostates manifesting PIN. Among PIN mice, 21 mice were removed during the study because of kidney tumors, bad health, change in MRI measurement protocol after first treatment or complications from intravenous cannulation and injection. Forty-five mice with PIN prostates were included in treatment groups 4−8 and were treated and followed up as intended. Figure 4 illustrates the time points at which mice were removed from the study.

Treatment effect on PD tumor volume

The therapeutic effect of Cab and Cab combined with US + MB was studied in TRAMP mice with PD tumors, and the tumor growth is illustrated in Figure 5. Twelve of 14 mice received all intended treatments. Mice were euthanized because of tumor burden (n = 8), bad health (n = 3) or air injection (n = 1). For the untreated controls, all tumors had an approximately logarithmic growth in volume. For the Cab group, three of four tumors decreased in size after treatment, but regrowth took place 2−6 wk after the last treatment. One tumor continued to grow despite treatment, but the

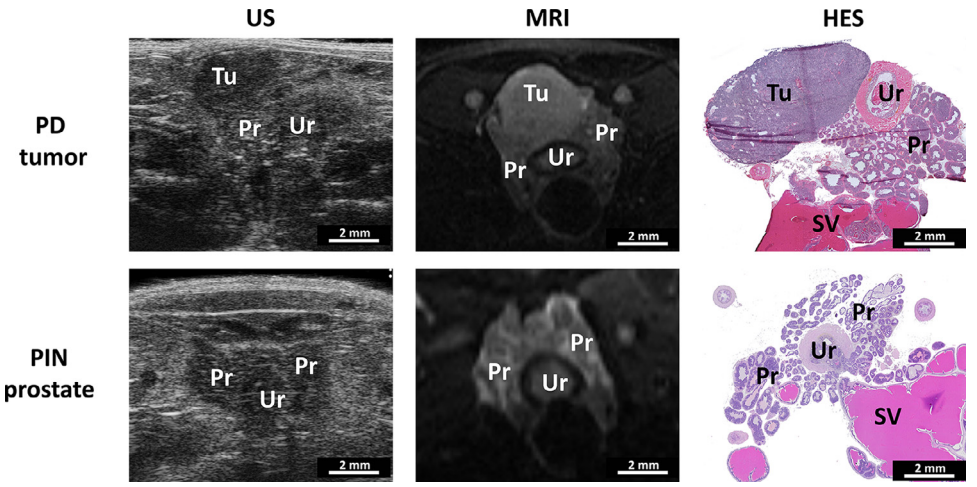

Fig. 3. Representative images of PD prostate tumors (top row) and prostates with PIN (bottom row) acquired with ultrasound imaging (left column), magnetic resonance imaging (middle column) and HES slide (right column). HES = hematoxylin, erythrosine and saffron; MRI = magnetic resonance imaging; PIN = prostatic intraepithelial neoplasia; PD = poorly differentiated; Pr = prostate; SV = seminal vesicle; Tu = tumor; Ur = urethra; US = ultrasound.

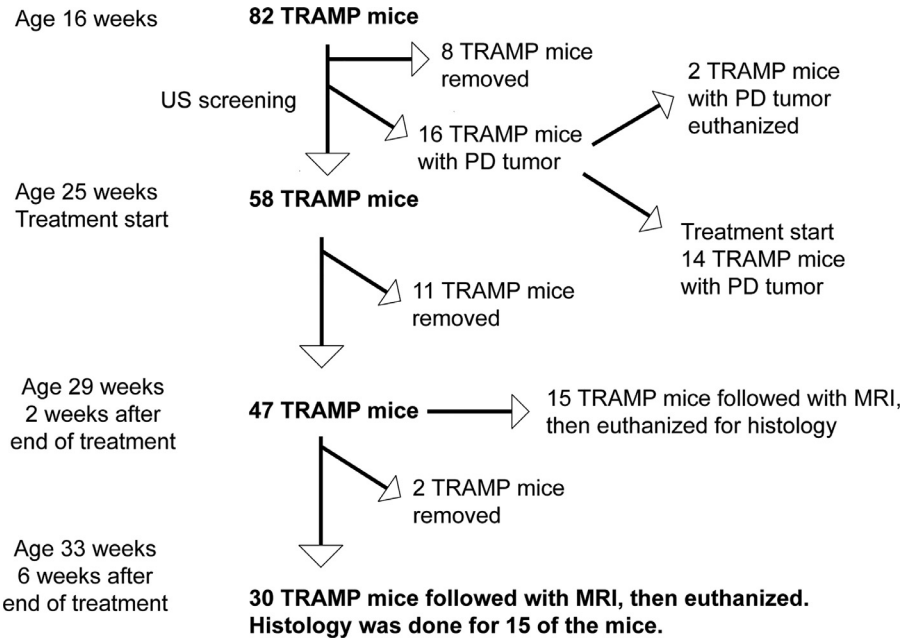

Fig. 4. Flow chart for recruitment of the two phenotypes of TRAMP mice to treatment studies. Fourteen mice with PD tumor and 45 mice with PIN prostate were treated and followed up as intended. PD = poorly differentiated; PIN = prostatic intraepithelial neoplasia, TRAMP = transgenic adenocarcinoma of the mouse prostate; US = ultrasound.

growth rate was less than that for the untreated controls. This tumor was approximately four times larger in volume compared with the other PD tumors at treatment start, which can explain the poor therapeutic response. In the US + MB group, all tumors decreased in size after treatment. One mouse survived 10 wk after treatment without tumor recurrence. The PD tumor could not be detected by MRI, in contrast to the other mice, in which PD tumors were still detectable. The mouse without recurrence was euthanized 10 wk after the end of treatment because of acute poor health. Necropsy revealed bowel necrosis. Among the other mice receiving US + MB treatment, one died during the last treatment because of unintended injection of air and another was euthanized because of weight loss 3 wk after the start of treatment.

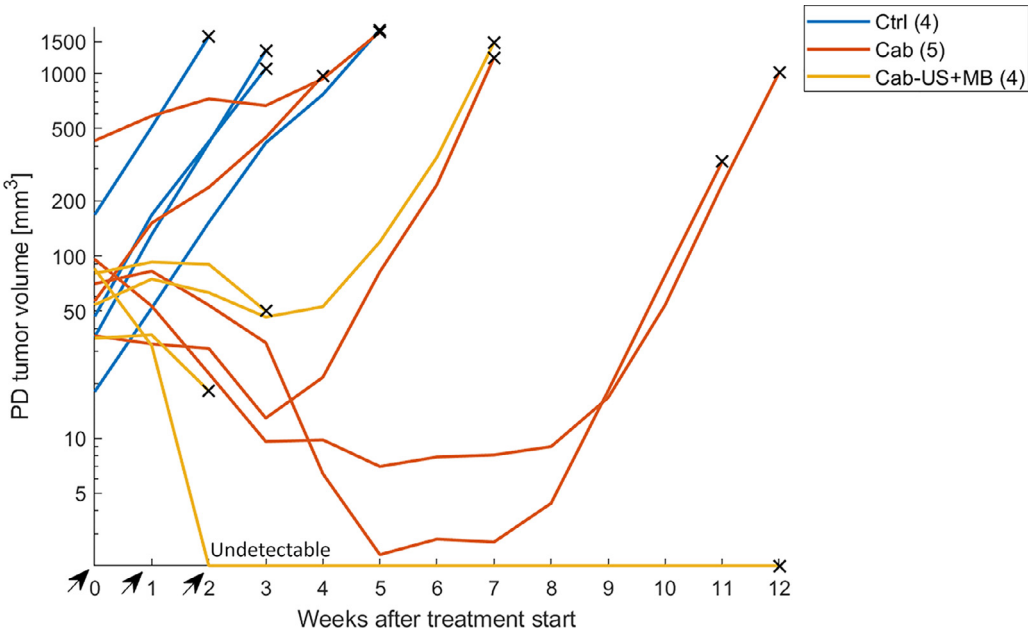

Fig. 5. Tumor volume (in mm^3) on a logarithmic axis as a function of time after start of treatment. Treatment was given in weeks 0, 1 and 2 (marked with *arrows*). The *colored lines* indicate tumor growth for individual mice. Time of euthanasia is marked with a *cross*. Ctrl = control; Cab = cabazitaxel; Cab−US + MB = cabazitaxel combined with therapeutic ultrasound and microbubbles.

Treatment effect on prostate volume

The treatment efficacy of Cab, Cab−US + MB, Cab-loaded NP and Cab-loaded NP with US + MB was assessed by determining the prostate volume of 45 mice (Fig. 6). Fifteen of the mice were euthanized for histology 2 wk after treatment, and 30 mice were followed for 4 more wk. Two weeks after end of treatment, the mean prostate volume had increased by 26% for the untreated control group, and for all treatment groups the mean prostate volume had decreased by 16%−18%. There was no significant difference between the different treatments. The mean prostate volume for all treated mice was significantly different from that for the untreated control group. Between 2 and 4 wk after treatment, mean prostate volume increased in all groups, and the growth rate was higher than in the untreated control group. Six weeks after end of treatment, there was no difference between mean prostate volumes of the different groups, including the untreated control. Large variations were observed between individual prostates, especially for the untreated controls (Supplementary Fig. S1, online only). For the untreated controls, prostate volume increased rapidly for 1 mouse, increased slowly for most of the mice and decreased for 2 mice. The variation was less for the mice treated with Cab, either free or encapsulated. The majority of the prostates decreased in volume during treatment (except in 2 mice given free Cab). For the prostates that were also treated with US + MB, the variation was even less, and all prostate volumes decreased during treatment.

Treatment effect on prostate histology scoring and proliferative index

Mice without PD tumor were euthanized either 2 or 6 wk after end of treatment, and prostates were harvested for analysis. HES sections were graded with the Berman−Booty scheme, and the Ki-67 sections were quantified based on the percentage of positive cells. Figure 7 illustrates representative HES and Ki-67 staining of TRAMP prostates and details of the ventral, lateral and dorsal prostate lobe. On HES-stained sections, the ventral prostate was characterized by multifocal low-grade PIN and not much change in the stroma compared with normal ventral prostate. The lateral and dorsal lobes expressed diffuse high-grade PIN. The lateral lobe's connective tissue had fibroblast invasion and collagen fibers surrounding the lobes, while the dorsal lobe had hypertrophic smooth muscle cells surrounding the glands. Cells positive for Ki-67 were typically epithelial cells located basally in the glands.

To obtain a quantitative number for the malignancy of the prostate, HES images were scored using the Berman−Booty grading scheme. The scores were similar for all groups and for the two time points (Fig. 8); that is, there was no clear difference between the treatment groups and untreated control. Most groups had one prostate with a higher or lower score compared with the majority. Only one sample was classified as malignant. This mouse was in the NP group and had PD tumor tissue in the ventral prostate, but the PD tumor was small

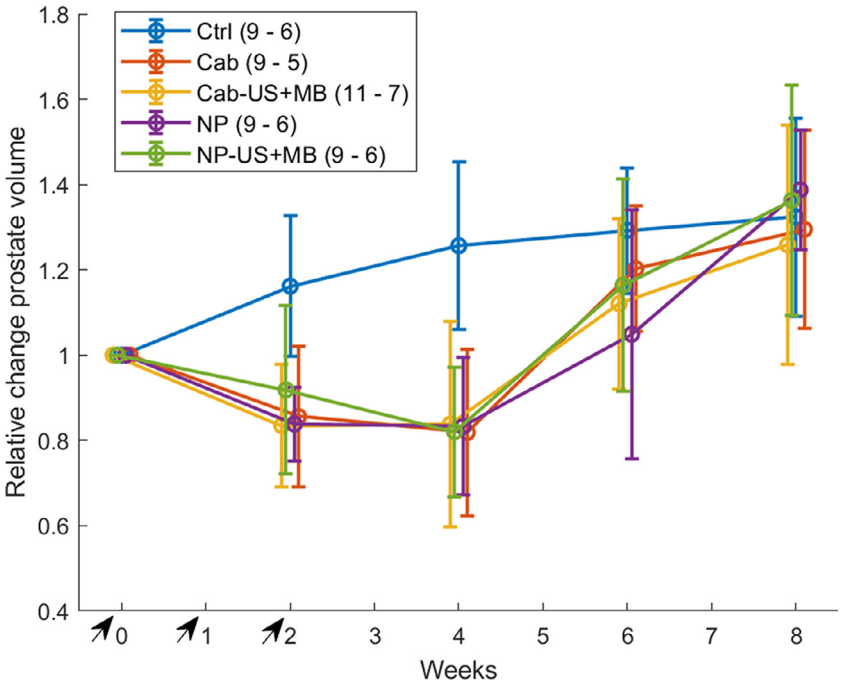

Fig. 6. Mice followed from before treatment until 8 wk after start of treatment. Relative prostate volume as a function of time after start of treatment. Treatment was given in weeks 0, 1 and 2 (marked with *arrows*). The *colored symbols* represent group means, and the *error bars,* standard deviations. Four weeks after the start of treatment, 15 mice were euthanized for histology and immunohistochemistry. The number of animals per group, before and after 4 wk after treatment, are given in the box. Ctrl = control; Cab= cabazitaxel; Cab−US + MB = cabazitaxel combined with therapeutic ultrasound and microbubbles; NP = cabazitaxel encapsulated in nanoparticles; NP−US + MB = cabazitaxel encapsulated in nanoparticles combined with therapeutic ultrasound and microbubbles.

and had not been detected during MRI. In general, the ventral prostates were homogenous, with most prostates scoring 8. This score was characterized by a multifocal distribution of cell stratification and crowding of epithelial cells. The lateral and dorsal prostate were especially homogenous, with most samples scoring 18, corresponding to a diffuse distribution of features like tall papillary projections filling the lumen and clusters of cells herniating into the surrounding smooth muscle.

The proliferative index was similar for all treatment groups (Fig. 8) although there was a large variation within the groups. For the ventral and lateral prostate, the proliferative index was lower 6 wk after treatment compared with 2 wk after treatment. The ventral lobe had the lowest proliferative activity with 10%−20% and 0−20% proliferative cells 2 and 6 wk after treatment, respectively. Cells in the lateral and dorsal lobes had higher proliferative activity, and the Ki-67 positive cells ranged from 0%−50% or from 10%−60% in the lateral and dorsal lobe, respectively. Staining with the proliferation marker Ki-67 was quite homogeneous in the ventral prostate lobe and heterogeneous for the lateral and dorsal lobe, corresponding to larger variation in proliferative index in the lateral and dorsal lobes compared with the ventral lobe.

NP and US + MB effect on Cab biodistribution

The biodistribution of Cab was assessed by MS quantification of Cab for samples harvested 2 h after treatment in mice without PD tumors (Fig. 9). Encapsulating Cab in NP enhanced the amount of Cab per milligram of organ in most organs, especially in spleen, liver and blood. Cab was not detected in the brain of any mouse. The blood concentration of free Cab was very low compared with that of NP-encapsulated Cab. Both nanograms of Cab per milligram of organ (Fig. 9a) and percentage of injected dose (Fig. 9c, 9d) are provided. The concentration of Cab in the prostate lobes was higher for NP groups than free Cab groups (Fig. 9b). The mice were perfused; thus, the increased uptake should be owing to extravasated NP or drugs, although it cannot be ruled out that some NP were left in the blood vessels.

Apnea after NP injection

All mice that received NP injections developed apnea and bradycardia immediately after injection. Data from four mice revealed a mean apnea duration of 40 s (range: 38−43 s). The mean duration from start of bradycardia until the heart rate was the same as before injection was 54 s, (range: 50−57 s). The mean heart rate before injection was 441 bpm, and the mean minimum

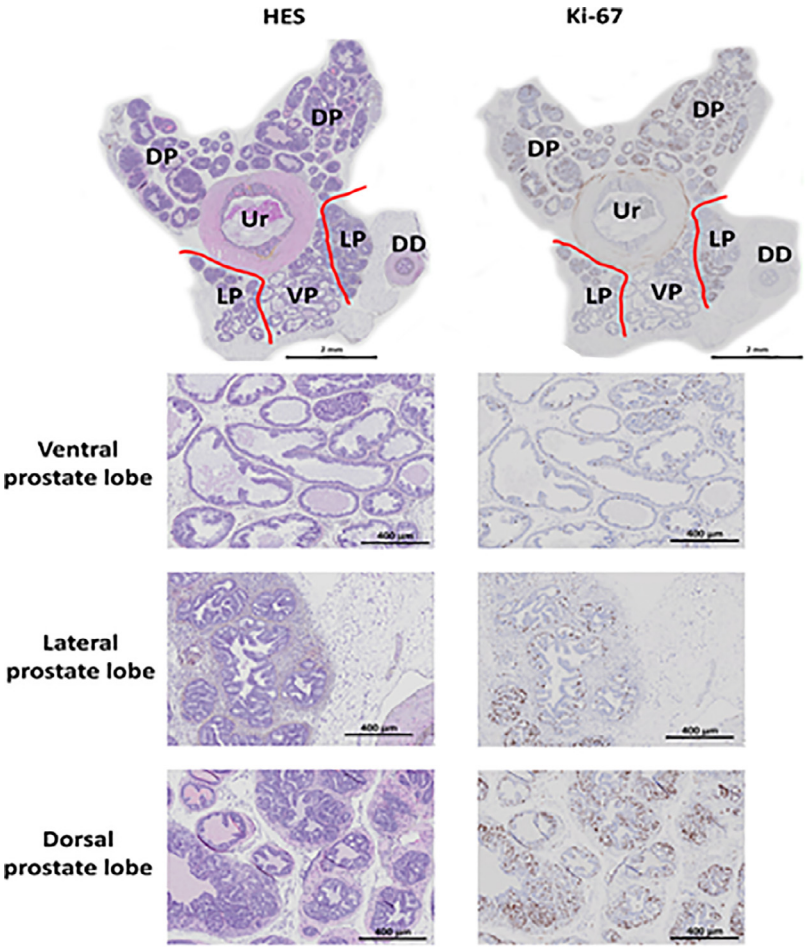

Fig. 7. On the left are HES-stained sections, and on the right, column Ki-67 stained sections. In the top row is an overview of the prostate; the other rows illustrate details of different prostate lobes. The images are representative of the most common lesions in the respective lobes: multifocal low-grade PIN in the ventral prostate lobe and diffuse high-grade PIN in the lateral and dorsal prostate lobe. DD = ductus deference; DP = dorsal prostate lobe; HES = hematoxylin, erythrosine and saffron; LP = lateral prostate lobe; VP = ventral prostate; Ur = urethra.

heart rate after injection was 109 bpm. No mice died from the intravenous NP injection.

Weight loss

Weight was assessed as a measure of toxicity and is illustrated in Supplementary Figure S2 (online only). There was no significant difference in weight between groups at the start of treatment. Two weeks after the end of treatment, the mean weight of the untreated control mice was unchanged, whereas the treated mice had a mean reduction in weight of 5%−7%. At this time point, the difference between the control group (0.0% mean change in weight) and the NP group (6.2% mean reduction in weight) and that between the control group and the NP−US + MB group (7.1% mean reduction in weight) were significant. Six weeks after the end of treatment, there was no significant difference in weight between the groups.

DISCUSSION

The treatment efficacy of Cab, either free of encapsulated in NP, in combination with US + MB treatment was evaluated in the TRAMP model. To our knowledge, such a study has not been published before in a spontaneous, orthotopic prostate cancer model. The rationale underlying this study was to verify the promising strategy of using NP and US + MB to improve the delivery of drugs (Snipstad et al. 2017, 2018) in a more clinically relevant model. Spontaneous orthotopic models are thought to represent human cancers more precisely than xenografts because mice from spontaneous cancer models are immunocompetent, have more heterogeneous tumor genetics and have organ-specific stroma around the cancer cells (Gengenbacher et al. 2017). The TRAMP model develops different phenotypes, which are probably

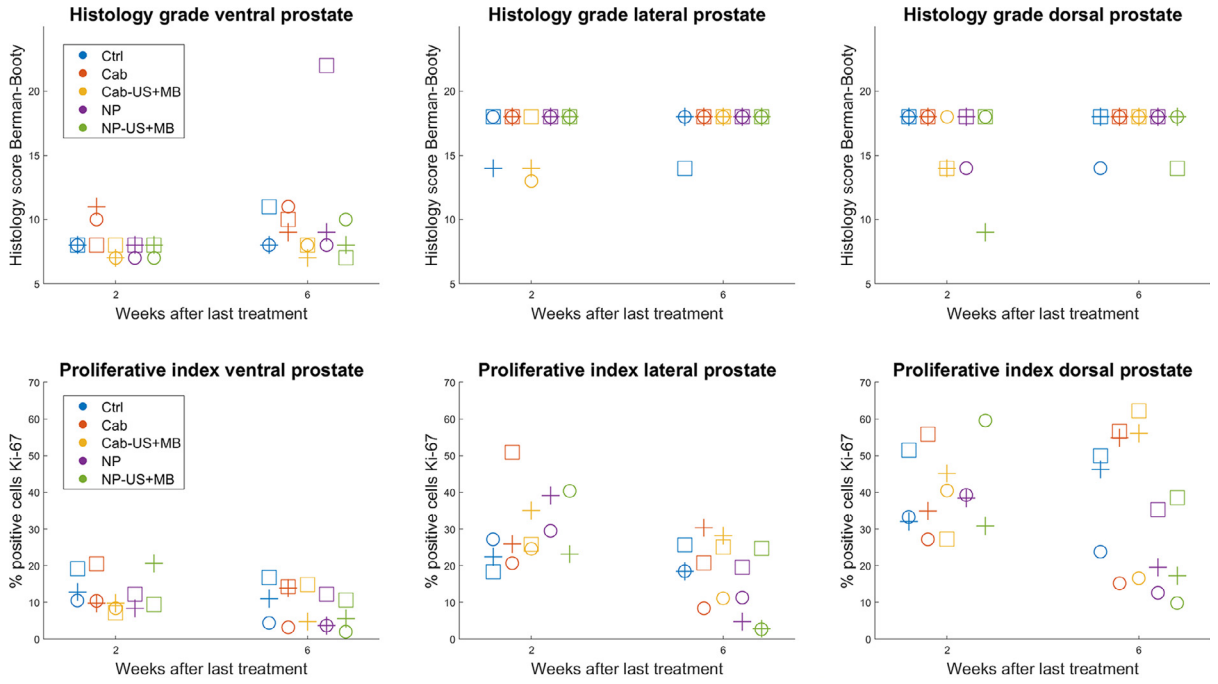

Fig. 8. In the top row is histology grading using the Berman−Booty grading system 2 and 6 wk after the last treatment for all different groups for three prostate lobes. In the bottom row are the proliferative indexes (percentage of positive Ki-67-stained cells) for three prostate lobes. Each symbol represents an individual mouse; some data points have perfect overlap.

representative of different types of human disease. Previous studies of TRAMP PD tumors have indicated that they are positive for IHC staining for synaptophysin, indicating a neuroendocrine (NE) phenotype (Chiaverotti et al. 2008). In human disease, prostate cancer with an NE phenotype is rare and carries a poor prognosis (Sun et al. 2009). However, as prostate cancer progresses, it sometimes differentiates into an NE phenotype in late stages of the disease. Studying the TRAMP PD NE phenotype might therefore afford insights into treatment of the aggressive NE phenotype or transformed late-stage adenocarcinoma (Grabowska et al. 2014).

Most mice in this study did not develop PD tumors, but prostate volumes increased compared with those of wild-type mice (Hill et al. 2016), and histology revealed high-grade PIN, classified by the Berman−Booty grading scheme. It has been argued that the dysplastic lesions in the TRAMP model do not progress to cancer and that PIN therefore is a misleading term because it implies a malignant potential (Chiaverotti et al. 2008). Generalizing from the non-tumor TRAMP mice to human disease is not straightforward because it is unclear if it progresses to malignant disease. Depending on the grading scheme used, it could be argued that we have treated a benign condition, a pre-malignant condition or a malignant disease.

Treatment effect on PD tumor volume

A subgroup of the TRAMP mice developed PD tumors, and the therapeutic efficacy of Cab and Cab combined with US + MB was studied. Because of small numbers of PD tumors, the effect of NP encapsulation was not assessed. All mice with PD tumors responded to Cab or Cab combined with US + MB either by reduction of growth rate or by reduction in PD tumor volume, indicating that Cab is an effective drug for PD tumors in the TRAMP model.

Degrassi et al. (2007) reported, in accordance with our study, that doxorubicin can reduce the volume of PD tumors in the TRAMP model. Degrassi et al. treated six mice with PD tumors with 7.5 mg/kg doxorubicin per week for 3 wk and monitored treatment response with MRI. All tumor volumes were reduced, but three tumors started growing again during 40 d of follow-up.

Treating the PD tumors with Cab combined with US + MB had effects similar to those of Cab alone, except for one PD tumor, which disappeared completely on MRI. However, the number of tumors is too small to conclude whether US + MB enhances the treatment effect of Cab. Still, the results are encouraging and are in line with observations using xenografts, where treating subcutaneous xenografts with drugs or NP combined with US + MB caused reduced tumor growth and even resulted in complete remission (Snipstad et al. 2017).

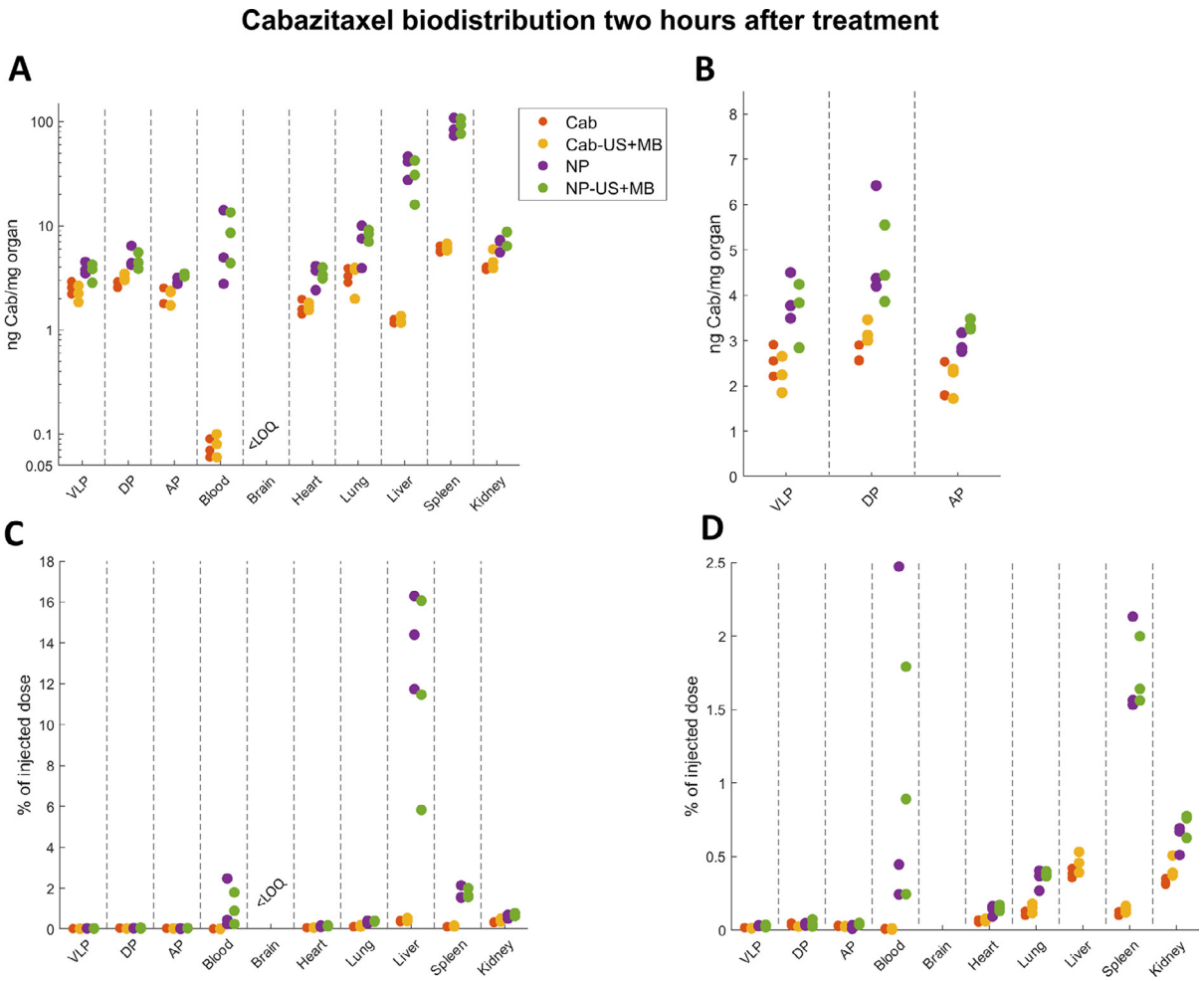

Fig. 9. (a) Amount (ng/mg organ) of cabazitaxel (Cab) on a logarithmic axis for all organs and blood. The data points represent measurements from organs of individual mice, three per treatment group. (b) Amount of Cab on a linear axis for the prostate lobes only. (c) Percentage of injected dose in all organs and blood. (d) Percentage of injected dose in all organs on a shorter axis to visualize differences between groups. APL = anterior prostate lobe; Cab = cabazitaxel; DPL = dorsal prostate lobe; LOQ = limit of quantification; VPLP = ventral and lateral prostate lobe.

The benefit of using US + MB is probably greatest in tumors where extravasation and penetration of drug through the extracellular matrix limit drug delivery. Sonopermeation is reported to be more effective in xenografts expressing low EPR than in xenografts with high EPR (Theek et al. 2016). Thus, sonopermeation depends on tumor physiology, such as the vascular network and the composition and structure of the extracellular matrix, which are known to vary between and within tumors. This can explain some of the variation in therapeutic responses to US + MB. The barriers for delivery of drugs and NP in PD tumors have not been well described. One multiparametric MRI study has indicated that as TRAMP lesions become PD, the vascular volume increases, oxygenation decreases and protein content increases (Ferrauto et al. 2018). However, it is not clear what impact such changes have on drug delivery.

Treatment effect on prostate

All treatments that included Cab significantly reduced prostate volume as compared with both the starting volume and the volume for the untreated controls. This might indicate that Cab, either free or encapsulated, extravasates and diffuses efficiently through the prostate tissue. Although a multiparametric MRI analysis of the TRAMP prostate has indicated that the perfusion is heterogenous and that the leakiness is slightly lower compared with that of an ovarian cancer xenograft (Kim et al. 2019), our results indicate that perfusion and vascular permeability are sufficient for successful delivery of free and encapsulated Cab. In the prostate, Cab and NP might not encounter the same barriers as in solid tumors, such as the high interstitial fluid pressure and dense stroma (Boucher et al. 1990; Netti et al. 2000; Eikenes et al. 2005). The observation that encapsulated

Cab is as efficient as free drug is promising, because encapsulating drugs has the potential to reduce toxicity from chemotherapeutic agents (Harris et al. 2002).

The US applied did not improve the therapeutic response. The US settings used were based on a study that reported very promising therapeutic results in subcutaneous breast cancer xenografts in mice (Snipstad et al. 2017). However, in the TRAMP mice, an increase in acoustic power or change in US pulses might be needed. Achieving a successful therapeutic response requires optimal US exposure (frequency, acoustic power, pulse length), which might be tumor and mouse dependent. Furthermore, using MB designed for drug delivery and not for imaging, such as SonoVue, might provide more successful results (Snipstad et al. 2018).

The mean prostate volume regrew beyond the pre-treatment volume in all treatment groups during the 6 wk after the last treatment. Because the prostate hyperplasia has a genetic cause that was not removed by the treatment, regrowth could be expected. Also, none of the mice were castrated; thus, testosterone would still stimulate the prostate tissue to grow. The results are consistent with the few comparable studies available: Degrassi et al. (2007) treated six TRAMP mice without tumors with 7.5 mg/kg doxorubicin weekly for 3 wk and monitored treatment response with volume measurements based on MRI. They also observed a clear reduction in prostate size initially and a regrowth after the end of treatment, outgrowing the pre-treatment size. Søgaard et al. (2018) treated the TRAMP mice with either docetaxel or docetaxel plus a peptide targeting the cellular scaffold protein, proliferating cell nuclear antigen; both groups receiving docetaxel had smaller prostate volumes than the control up to 4 wk after one treatment with 3 mg/kg docetaxel.

Histology grading and Ki-67 staining were done to assess treatment effects on the microscopic level. Neither histology grading nor Ki-67 staining revealed any difference between treatment groups and no difference between the two time points (2 and 6 wk after treatment). If there was a transient effect from treatment, 2 and 6 wk might be too late to detect any change. Several studies on prevention of cancer in the TRAMP model have reported reduction in the expression of Ki-67 in the model, for example, through administration of the flavone apigenin (Shukla et al. 2014) and an energy restriction mimetic agent (Berman-Booty et al. 2013). However, these studies assess the preventive effect of treatment and begin at a young age, treat for a long time and often euthanize while therapy is ongoing.

Biodistribution

Improved therapeutic response requires improved uptake of the drug in the tumor and in neoplastic cells. Thus, prostate uptake of free and encapsulated Cab and biodistribution in various organs were quantified with MS. Encapsulation of Cab in NP had a clear effect on blood concentration and biodistribution 2 h after intravenous administration. These results are in line with previous work on the biodistribution of the poly(2-ethyl-butyl cyanoacrylate) (PEBCA) NP (Snipstad et al. 2017; Fusser et al. 2019). The lungs also had increased levels of Cab when it was encapsulated in NP; however, as the lungs were not perfused with PBS, making it is difficult to separate the contribution from Cab in blood from that of Cab in lung tissue. Regardless of US + MB treatment, mice treated with Cab encapsulated in NP had a higher Cab content in the different prostate lobes compared with mice treated with free Cab. The approximately 1.7 times higher uptake for NP-encapsulated Cab compared with free Cab, comparing the two treatment groups, was not sufficient for any detectable therapeutic improvement. Possible mechanisms for the higher uptake of encapsulated Cab are longer circulation time, lower distribution volume and slower excretion. US + MB did not have any clear effect on prostate uptake for free Cab or Cab encapsulated in NP.

Toxicity

Throughout the study, injection of NP led to transient apnea and bradycardia in the TRAMP mice. The apnea and bradycardia usually occurred simultaneously, which could indicate a reflex-mediated response. The Bezold−Jarish reflex is known to have this effect in mice, and can be triggered by different stimuli, both chemical and mechanical (Campagna and Carter 2003). However, in previous studies in female Balb/c nude mice, the injection of the same polymeric NP did not lead to transient apnea (Snipstad et al. 2017; Fusser et al. 2019). Further investigation is needed to determine the cause of the apnea and bradycardia in the TRAMP mice. Clinical studies have indicated that pulmonary disease is an important concern in clinical studies with polymeric NP. In a phase II clinical trial with Doxorubicin-Transdrug, a polymeric nanoformulation of doxorubicin using the PEBCA polymer, 4 of 17 patients developed acute respiratory distress syndrome, and 3 of them died (Merle et al. 2017).

Mice in all groups receiving free Cab or NP lost weight during the treatment period. The mean weight loss for the treated groups was 5%−7%. Fusser et al. (2019) reported a weight loss of around 15% after two treatments of 15 mg/kg of Cab, either free or encapsulated, injected 3 d apart in female athymic nude foxn1^{nu} mice. Snipstad et al. (2017) treated female Balb/c nude mice with NP-encapsulated Cab, 10 mg/kg weekly for 2 wk, which caused no weight loss. Weight loss caused by Cab might be dependent on the mouse

model, and 10 mg/kg weekly might be close to the maximum dose tolerated in the TRAMP model.

CONCLUSIONS

Cab reduced PD tumor and prostate volume in the TRAMP model, but the effect was transient, and regrowth beyond pre-treatment volume took place after the end of treatment. The study did not find any clear added therapeutic efficacy from combining encapsulating Cab in NP or by using US + MB. These results differ from previous studies in xenograft models that reported an improved treatment response with NP encapsulation and US + MB treatment. We did not see any effect on histology grading and proliferation marker staining 2 and 6 wk after treatment. Quantification of Cab by MS revealed a clear increase in Cab concentration in blood, liver and spleen from encapsulating Cab in NP and a smaller increase in the prostate. The US applied was based on a previous successful study in subcutaneous xenografts, and optimal US parameters for the TRAMP model might be different. Thus, optimization of US parameters for TRAMP might give improved results.

Acknowledgments—We acknowledge the guidance from consultant pathologist Sverre Helge Torp in examining slides from the TRAMP mice. We acknowledge the support from and the use of the following infrastructures: Animal breeding, housing and genotyping were provided by the Comparative Medicine Core Facility (CoMed). Histology and immunohistochemistry sectioning and staining were performed at the Cellular and Molecular Imaging Core Facility (CMIC). CoMed and CMIC are both at the Norwegian University of Science and Technology (NTNU) and are funded by the Faculty of Medicine at NTNU and Central Norway Regional Health Authority. MRI was performed at the MR core facility at the Norwegian University of Science and Technology. Equipment for therapeutic US was provided by The Norwegian Centre for Minimally Invasive Image Guided Therapy and Medical Technologies (NorMIT). We also acknowledge Yrr Mørch and Anne Hatletveit at SINTEF Industry for providing NP and guidance. MS analysis was also performed at SINTEF Industry. The project was supported by the Research Council of Norway (Project No. 240316), the Norwegian Cancer Society (Grant No. 6824920-2015) and the Central Norway Regional Health Authority (Grant No. 90059700).

Conflict of Interest—There are no conflict of interest.

SUPPLEMENTARY MATERIALS

Supplementary material associated with this article can be found in the online version at doi:10.1016/j.ultrasmedbio.2020.07.004.

REFERENCES

Bankhead P, Loughrey MB, Fernández JA, Dombrowski Y, McArt DG, Dunne PD, McQuaid S, Gray RT, Murray LJ, Coleman HG, James JA, Salto-Tellez M, Hamilton PW. QuPath: Open source software for digital pathology image analysis. Sci Rep 2017;7:16878.

Berman-Booty LD, Sargeant AM, Rosol TJ, Rengel RC, Clinton SK, Chen CS, Kulp SK. A review of the existing grading schemes and a proposal for a modified grading scheme for prostatic lesions in TRAMP mice. Toxicol Pathol 2012;40:5–17.

Berman-Booty LD, Chu PC, Thomas-Ahner JM, Bolon B, Wang D, Yang T, Clinton SK, Kulp SK, Chen CS. Suppression of prostate epithelial proliferation and intraprostatic progrowth signaling in transgenic mice by a new energy restriction-mimetic agent. Cancer Prev Res (Phila) 2013;6:232–241.

Boucher Y, Baxter LT, Jain RK. Interstitial pressure gradients in tissue-isolated and subcutaneous tumors: Implications for therapy. Cancer Res 1990;50:4478–4484.

Campagna JA, Carter C. Clinical relevance of the Bezold−Jarisch reflex. Anesthesiology 2003;98:1250–1260.

Carpentier A, Canney M, Vignot A, Reina V, Beccaria K, Horodyckid C, Karachi C, Leclercq D, Lafon C, Chapelon JY, Capelle L, Cornu P, Sanson M, Hoang-Xuan K, Delattre JY, Idbaih A. Clinical trial of blood-brain barrier disruption by pulsed ultrasound. Sci Transl Med 2016;8 343.re2.

Chiaverotti T, Couto SS, Donjacour A, Mao JH, Nagase H, Cardiff RD, Cunha GR, Balmain A. Dissociation of epithelial and neuroendocrine carcinoma lineages in the transgenic adenocarcinoma of mouse prostate model of prostate cancer. Am J Pathol 2008;172:236–246.

da Silva RF, Banzato TP, Alves LF, Carvalho JE, Agarwal R, Cagnon VHA. Antiangiogenic therapy with nintedanib affects hypoxia, angiogenesis and apoptosis in the ventral prostate of TRAMP animals. Cell Tissue Res 2020;379:407–420.

Day CP, Merlino G, Van Dyke T. Preclinical mouse cancer models: A maze of opportunities and challenges. Cell 2015;163:39–53.

Degrassi A, Russo M, Scanziani E, Giusti A, Ceruti R, Texido G, Pesenti E. Magnetic resonance imaging and histopathological characterization of prostate tumors in TRAMP mice as model for preclinical trials. Prostate 2007;67:396–404.

Dimcevski G, Kotopoulis S, Bjanes T, Hoem D, Schjott J, Gjertsen BT, Biermann M, Molven A, Sorbye H, McCormack E, Postema M, Gilja OH. A human clinical trial using ultrasound and microbubbles to enhance gemcitabine treatment of inoperable pancreatic cancer. Journal Control Release 2016;243:172–181.

Ding J, Chen J, Gao L, Jiang Z, Zhang Y, Li M, Xiao Q, Lee SS, Chen X. Engineered nanomedicines with enhanced tumor penetration. Nano Today 2019;29 100800.

Eikenes L, Tari M, Tufto I, Bruland OS, de Lange Davies C. Hyaluronidase induces a transcapillary pressure gradient and improves the distribution and uptake of liposomal doxorubicin (Caelyx) in human osteosarcoma xenografts. Br J Cancer 2005;93:81–88.

Fagerland ST, Hill DK, van Wamel A, de Lange Davies C, Kim J. Ultrasound and magnetic resonance imaging for group stratification and treatment monitoring in the transgenic adenocarcinoma of the mouse prostate model. Prostate 2020;80:186–197.

Ferlay J, Colombet M, Soerjomataram I, Dyba T, Randi G, Bettio M, Gavin A, Visser O, Bray F. Cancer incidence and mortality patterns in Europe: Estimates for 40 countries and 25 major cancers in 2018. Eur J Cancer 2018;103:356–387.

Ferrauto G, Di Gregorio E, Lanzardo S, Ciolli L, Iezzi M, Aime S. Generation of multiparametric MRI maps by using Gd-labelled-RBCs reveals phenotypes and stages of murine prostate cancer. Sci Rep 2018;8:10567.

Fusser M, Overbye A, Pandya AD, Morch Y, Borgos SE, Kildal W, Snipstad S, Sulheim E, Fleten KG, Askautrud HA, Engebraaten O, Flatmark K, Iversen TG, Sandvig K, Skotland T, Maelandsmo GM. Cabazitaxel-loaded poly(2-ethylbutyl cyanoacrylate) nanoparticles improve treatment efficacy in a patient derived breast cancer xenograft. J Control Release 2019;293:183–192.

Gengenbacher N, Singhal M, Augustin HG. Preclinical mouse solid tumour models: Status quo, challenges and perspectives. Nat Rev. Cancer 2017;17:751–765.

Gingrich JR, Barrios RJ, Morton RA, Boyce BF, DeMayo FJ, Finegold MJ, Angelopoulou R, Rosen JM, Greenberg NM. Metastatic prostate cancer in a transgenic mouse. Cancer Res 1996;56:4096–40102.

Grabowska MM, DeGraff DJ, Yu X, Jin RJ, Chen Z, Borowsky AD, Matusik RJ. Mouse models of prostate cancer: Picking the best model for the question. Cancer Metastasis Rev 2014;33:377–397.

Greenberg NM, DeMayo F, Finegold MJ, Medina D, Tilley WD, Aspinall JO, Cunha GR, Donjacour AA, Matusik RJ, Rosen JM. Prostate cancer in a transgenic mouse. Proc Natl Acad Sci USA 1995;92:3439–3443.

Harris L, Batist G, Belt R, Rovira D, Navari R, Azarnia N, Welles L, Winer E. Liposome-encapsulated doxorubicin compared with conventional doxorubicin in a randomized multicenter trial as first-line therapy of metastatic breast carcinoma. Cancer 2002;94:25–36.

Hill DK, Kim E, Teruel JR, Jamin Y, Wideroe M, Sogaard CD, Storkersen O, Rodrigues DN, Heindl A, Yuan Y, Bathen TF, Moestue SA. Diffusion-weighted MRI for early detection and characterization of prostate cancer in the transgenic adenocarcinoma of the mouse prostate model. J Magn Reson Imaging 2016;43:1207–1217.

Kim J, Moestue SA, Bathen TF, Kim E. R2* relaxation affects pharmacokinetic analysis of dynamic contrast-enhanced MRI in cancer and underestimates treatment response at 7 T. Tomography 2019;5: 308–319.

Kotopoulis S, Delalande A, Popa M, Mamaeva V, Dimcevski G, Gilja OH, Postema M, Gjertsen BT, McCormack E. Sonoporation-enhanced chemotherapy significantly reduces primary tumour burden in an orthotopic pancreatic cancer xenograft. Mol Imaging Biol 2014;16:53–62.

Lammers T, Kiessling F, Hennink WE, Storm G. Drug targeting to tumors: Principles, pitfalls and (pre-) clinical progress. J Control Release 2012;161:175–187.

Lin CY, Li JR, Tseng HC, Wu MF, Lin WL. Enhancement of focused ultrasound with microbubbles on the treatments of anticancer nanodrug in mouse tumors. Nanomed Nanotechnol Biol Med 2012;8: 900–907.

Liu Y, Wu X, Jiang H. Combined maternal and post-weaning high fat diet inhibits male offspring's prostate cancer tumorigenesis in transgenic adenocarcinoma of mouse prostate model. Prostate 2019;79:544–553.

Maeda H, Wu J, Sawa T, Matsumura Y, Hori K. Tumor vascular permeability and the EPR effect in macromolecular therapeutics: A review. J Controlled Release 2000;65:271–284.

Mainprize T, Lipsman N, Huang Y, Meng Y, Bethune A, Ironside S, Heyn C, Alkins R, Trudeau M, Sahgal A, Perry J, Hynynen K. Blood-brain barrier opening in primary brain tumors with non-invasive MR-guided focused ultrasound: A clinical safety and feasibility study. Sci Rep 2019;9:321.

Merle P, Camus P, Abergel A, Pageaux GP, Masliah C, Bronowicki JP, Zarski JP, Pelletier G, Bouattour M, Farloux L, Dorval E, verset G, Si-Ahmed S-N, Doffoel M, Couzigou P, Taieb J, Vasseur B, Attali P. Safety and efficacy of intra-arterial hepatic chemotherapy with doxorubicin-loaded nanoparticles in hepatocellular carcinoma. ESMO Open 2017;2 e000238.

Netti PA, Berk DA, Swartz MA, Grodzinsky AJ, Jain RK. Role of extracellular matrix assembly in interstitial transport in solid tumors. Cancer Res 2000;60:2497–2503.

Parisotto M, Metzger D. Genetically engineered mouse models of prostate cancer. Mol Oncol 2013;7:190–205.

Peer D, Karp JM, Hong S, Farokhzad OC, Margalit R, Langer R. Nanocarriers as an emerging platform for cancer therapy. Nat Nanotechnol 2007;2:751–760.

Raina K, Rajamanickam S, Singh RP, Deep G, Chittezhath M, Agarwal R. Stage-specific inhibitory effects and associated mechanisms of silibinin on tumor progression and metastasis in transgenic adenocarcinoma of the mouse prostate model. Cancer Res 2008;68:6822–6830.

Rosenblum D, Joshi N, Tao W, Karp JM, Peer D. Progress and challenges towards targeted delivery of cancer therapeutics. Nat Commun 2018;9 1410−1410.

Schindelin J, Arganda-Carreras I, Frise E, Kaynig V, Longair M, Pietzsch T, Preibisch S, Rueden C, Saalfeld S, Schmid B, Tinevez JY, White DJ, Hartenstein V, Eliceiri K, Tomancak P, Cardona A. Fiji: An open-source platform for biological-image analysis. Nat Methods 2012;9:676–682.

Shukla S, Bhaskaran N, Babcook MA, Fu P, Maclennan GT, Gupta S. Apigenin inhibits prostate cancer progression in TRAMP mice via targeting PI3 K/Akt/FoxO pathway. Carcinogenesis 2014;35:452–460.

Silva RS, Kido LA, Montico F, Vendramini-Costa DB, Pilli RA, Cagnon VHA. Steroidal hormone and morphological responses in the prostate anterior lobe in different cancer grades after celecoxib and goniothalamin treatments in TRAMP mice. Cell Biol Int 2018;42:1006–1020.

Sindhwani S, Syed AM, Ngai J, Kingston BR, Maiorino L, Rothschild J, MacMillan P, Zhang Y, Rajesh NU, Hoang T, Wu JLY, Wilhelm S, Zilman A, Gadde S, Sulaiman A, Ouyang B, Lin Z, Wang L, Egeblad M, Chan WCW. The entry of nanoparticles into solid tumours. Nat Mater 2020;19:566–575.

Snipstad S, Berg S, Morch Y, Bjorkoy A, Sulheim E, Hansen R, Grimstad I, van Wamel A, Maaland AF, Torp SH, Davies CL. Ultrasound improves the delivery and therapeutic effect of nanoparticle-stabilized microbubbles in breast cancer xenografts. Ultrasound Med Biol 2017;43:2651–2669.

Snipstad S, Sulheim E, de Lange Davies C, Moonen C, Storm G, Kiessling F, Schmid R, Lammers T. Sonopermeation to improve drug delivery to tumors: From fundamental understanding to clinical translation. Expert Opin Drug Deliv 2018;15:1249–1261.

Sogaard CK, Moestue SA, Rye MB, Kim J, Nepal A, Liabakk NB, Bachke S, Bathen TF, Otterlei M, Hill DK. APIM-peptide targeting PCNA improves the efficacy of docetaxel treatment in the TRAMP mouse model of prostate cancer. Oncotarget 2018;9:11752–11766.

Sulheim E, Morch Y, Snipstad S, Borgos SE, Miletic H, Bjerkvig R, Davies CL, Aslund AKO. Therapeutic effect of cabazitaxel and blood-brain barrier opening in a patient-derived glioblastoma model. Nanotheranostics 2019;3:103–112.

Sun Y, Niu J, Huang J. Neuroendocrine differentiation in prostate cancer. Am J Transl Res 2009;1:148–162.

Tharkar P, Varanasi R, Wong WSF, Jin CT, Chrzanowski W. Nano-enhanced drug delivery and therapeutic ultrasound for cancer treatment and beyond. Front Bioeng Biotechnol 2019;7:324.

Theek B, Baues M, Ojha T, Mockel D, Veettil SK, Steitz J, van Bloois L, Storm G, Kiessling F, Lammers T. Sonoporation enhances liposome accumulation and penetration in tumors with low EPR. J Controlled Release 2016;231:77–85.

Wang L, Bonorden MJ, Li GX, Lee HJ, Hu H, Zhang Y, Liao JD, Cleary MP, Lu J. Methyl-selenium compounds inhibit prostate carcinogenesis in the transgenic adenocarcinoma of mouse prostate model with survival benefit. Cancer Prev Res 2009;2:484–495.

Wang Y, Li Y, Yan K, Shen L, Yang W, Gong J, Ding K. Clinical study of ultrasound and microbubbles for enhancing chemotherapeutic sensitivity of malignant tumors in digestive system. Chin J Cancer Res 2018;30:553–563.

Wilhelm S, Tavares AJ, Dai Q, Ohta S, Audet J, Dvorak HF, Chan WCW. Analysis of nanoparticle delivery to tumours. Nat Rev Mater 2016;1:16014.

Zitvogel L, Pitt JM, Daillère R, Smyth MJ, Kroemer G. Mouse models in oncoimmunology. Nat Rev Cancer 2016;16:759–773.